HHS Public Access

Author manuscript

Mucosal Immunol. Author manuscript; available in PMC 2024 June 17.

Published in final edited form as:

Mucosal Immunol. 2024 June ; 17(3): 476–490. doi:10.1016/j.mucimm.2023.12.004.

PD-1 signaling in neonates restrains CD8+ T cell function and protects against respiratory viral immunopathology

Taylor Eddens[1,2], **Olivia B. Parks**[3], **Yu Zhang**[4], **Michelle L. Manni**[5], **Jean-Laurent Casanova**[6,7,8,9,10], **Masato Ogishi**[8], **John V. Williams**[2,4,*]

[1]UPMC Children's Hospital of Pittsburgh Allergy/Immunology Division, Pittsburgh, PA, USA

[2]University of Pittsburgh School of Medicine, Department of Pediatrics, Pittsburgh, PA, USA

[3]University of Pittsburgh Medical Scientist Training Program, Pittsburgh, PA, USA

[4]Institute for Infection, Inflammation, and Immunity in Children (i4Kids), Pittsburgh, PA, USA

[5]Division of Pulmonary Medicine, UPMC Children's Hospital of Pittsburgh, Pittsburgh, PA, USA

[6]Laboratory of Human Genetics of Infectious Diseases, Necker Branch, Institut National de la Santé et de la Recherche Médicale (INSERM) U1163, Necker Hospital for Sick Children, Paris, France.

[7]University Paris Cité, Imagine Institute, Paris, France.

[8]St. Giles Laboratory of Human Genetics of Infectious Diseases, Rockefeller Branch, Rockefeller University, New York, NY, USA.

[9]Howard Hughes Medical Institute, New York, NY, USA.

[10]Department of Pediatrics, Necker Hospital for Sick Children, Paris, France.

Abstract

Respiratory viral infections, including human metapneumovirus (HMPV), remain a leading cause of morbidity and mortality in neonates and infants. However, the mechanisms behind the increased sensitivity to those respiratory viral infections in neonates are poorly understood. Neonates, unlike adults, have several anti-inflammatory mechanisms in the lung, including elevated baseline expression of PD-L1, a ligand for the inhibitory receptor PD-1. We thus hypothesized that neonates would rely on PD-1:PD-L1 signaling to restrain antiviral CD8 responses. To test this, we developed a neonatal primary HMPV infection model using WT C57BL/6 (B6) and *Pdcd1*$^{-/-}$ (lacking PD-1) mice. HMPV-infected neonatal mice had increased PD-L1/PD-L2 co-expression on innate immune cells, but similar number of antigen-specific CD8^{+} T cells and upregulation of

*Corresponding Author: John V. Williams, 4401 Penn Avenue, Rangos Research Building 9122, Pittsburgh, PA 15224, jvw@pitt.edu.

Author Contributions: T.E.- designed and performed experiments, analyzed data, and wrote manuscript. O.B.P.- performed and assisted with experiments, revised manuscript. Y.Z.- contributed analytic tools, revised manuscript. M.L.M.- contributed analytic tools, revised manuscript. M.O./J.L.C.- provided and analyzed human data. J.V.W.- provided mentorship and funding for project, revised manuscript.

Competing Interest Statement: JVW previously served on SAB for Quidel and Independent Data Monitoring Board for GlaxoSmithKline. All other authors declare no conflict of interest.

Disclosures: The authors did not use generative AI for any text within this manuscript.

PD-1 compared to adult B6 mice. Neonatal $CD8^+$ T cells had reduced IFN-γ, granzyme B, and IL-2 production compared to B6 adults. *Pdcd1*$^{-/-}$ neonatal $CD8^+$ T cells had markedly increased production of IFN-γ and granzyme B compared to B6 neonates. *Pdcd1*$^{-/-}$ neonates had increased acute pathology with HMPV or influenza. *Pdcd1*$^{-/-}$ neonates infected with HMPV had long-term changes in pulmonary physiology with evidence of immunopathology and a persistent $CD8^+$ T cell response with increased granzyme B production. Using single cell RNA sequencing from a child lacking PD-1 signaling, a similar activated $CD8^+$ T cell signature with increased granzyme B expression was observed. These data demonstrate that PD-1 signaling critically limits $CD8^+$ T cell effector functions and prevents immunopathology in response to neonatal respiratory viral infections.

1.1 Introduction

Lower respiratory tract infections (LRTI) remain the leading infectious cause of mortality worldwide in children <5 years.[1] Viruses are major contributors to this high mortality, as respiratory syncytial virus (RSV), human metapneumovirus (HMPV), and influenza virus account for an estimated 164,500 deaths per year globally in children under 5.[2-4] Moreover, RSV, HMPV, and influenza cause 33.1 million, 14.2 million, and 10.1 million LRTI annual cases, respectively.[2-4] While this staggering global burden includes all children under 5, additional studies have demonstrated that infants and children born prematurely have worse outcomes associated with viral LRTIs, including increased mortality.[2-9]

Neonatal and infant lungs are uniquely susceptible to worse respiratory virus infection outcomes. The neonatal lung is still actively developing and undergoes further alveolarization for 30 days in mice and 2 years in humans.[10] Moreover, the immunologic milieu in the neonatal lung is vastly different than the adult lung.[11,12] For example, pro-inflammatory innate responses are dampened and innate cells provide limited co-stimulatory help to adaptive cells.[13-20] Further, PD-L1, a ligand for the inhibitory receptor PD-1, is upregulated shortly after birth and contributes towards a tolerogenic skewing of the adaptive compartment in response to airway microbiota.[21]

PD-1:PD-L1 signaling limits $CD8^+$ T cell responses to respiratory viral infections. Human bronchial epithelial cells upregulated PD-L1 expression following RSV infection and blockade of PD-L1 in that co-culture model led to increased $CD8^+$ T cell effector functions.[22] In murine models of HMPV and influenza, PD-1 was markedly upregulated on pulmonary antigen-specific $CD8^+$ T cells over the course of infection.[23,24] Disruption of PD-1:PD-L1 signaling by antibody blockade or genetic ablation led to increased degranulation and production of IFN-γ by $CD8^+$ T cells, increased viral clearance, and decreased weight loss in the HMPV murine model. [24,25] In contrast, while adult mice infected with RSV had induction of PD-1 expression on $CD8^+$ T cells, blockade of PD-L1 led to enhanced morbidity with no discernible difference in viral clearance.[26] Collectively, these studies demonstrate a critical role for the PD-1:PD-L1 axis in constraining effector function of $CD8^+$ T cells against acute respiratory viral infections. However, the neonatal response to HMPV and role of PD-1:PD-L1 signaling in dictating $CD8^+$ T cell function has been poorly studied.

We hypothesized that PD-1:PD-L1 signaling would be critical in response to respiratory viral infections in neonatal mice. To test this hypothesis, we developed a neonatal model of HMPV and discovered increased expression of PD-1 on CD8+ T cells along with PD-L1/PD-L2 upregulation on multiple immune cell types following infection. Additionally, we found PD-1 upregulation on antigen-specific neonatal $CD8^+$ T cells, which limited effector functions. However, while disruption of PD-1:PD-L1 signaling increased $CD8^+$ functionality, this led to enhanced HMPV-associated histopathology and increased mortality among influenza-infected neonates. Analysis of single-cell RNAseq data from a child lacking PD-1 who died of pulmonary autoimmunity revealed a similar transcriptional signature. Collectively, these data suggest that inhibition of neonatal $CD8^+$ T cells by PD-1:PD-L1 signaling is critical to limit immunopathology following respiratory viral infection.

1.2. Results

1.2.1. Neonatal mice are permissive for and resolve HMPV infection

Neonatal mice were infected intranasally with $2.8x10^6$ PFU of HMPV on day of life 4-6, using a similar inoculating dose as a previously established neonatal RSV model.[27] HMPV-infected pups had a significantly reduced rate of weight gain when compared to mock infected co-housed controls (Fig. 1A). Intranasal inoculation with HMPV was efficient, as a high titer HMPV could be recovered in the lungs immediately after infection (**day 0,** Fig. 1B). Viral burden then plateaued at day 3 post-infection followed by a second peak at day 5, consistent with an eclipse phase (Fig. 1B). HMPV was then rapidly cleared, with all mice having undetectable viral burden by day 8 post-infection (Fig. 1B). Histologic assessment revealed diffuse interstitial inflammation with cellular recruitment by day 2 post-infection, perivascular and peribronchial cellular infiltration by day 5 post-infection (Fig. 1C). Quantification of alveolar septal wall thickness demonstrated increased interstitial inflammation at days 2 and 5 post-HMPV infection (Fig. 1D). Lymphocytic clusters emerged in HMPV-infected animals by day 7 post-infection (Figs. 1C, 1E). To define transmission and transplacental immunity in this model, we observed that repeated litters had similar burdens of infection, while direct maternal infection provided protective immunity consistent with transplacental transfer of antibody (Fig. S4). These data suggest that inoculation of pups with HMPV does not lead to direct infection of the dams, which allows for repeated use of breeder pairs (Fig. S4). Collectively, these data demonstrate a reproducible model of HMPV infection in neonatal mice.

1.2.2. Upregulation of PD-L1 following neonatal HMPV infection

Neonatal mice have been previously shown to upregulate PD-L1 on dendritic cells under homeostatic conditions in the lung.[21] Given this baseline difference, we sought to characterize PD-1 ligand expression (e.g. PD-L1 and PD-L2) expression following HMPV infection. Both neonatal and adult mice had increased PD-L1 protein quantity in lung homogenate at day 1 post-HMPV infection compared to age-matched controls, while PD-L2 protein was below the limit of detection in all groups (Fig. S5A). At day one post-HMPV infection, both neonates and adults upregulated PD-L1 on $CD45^+$ leukocytes as measured by percent, total cell number, and mean fluorescence intensity (MFI) (Fig. 2A-D). Interestingly,

neonates had a baseline PD-L1^{+}PD-L2^{+} CD45^{+} population, which was sustained following infection (Fig. 2A-C). Adult mice had significantly fewer PD-L1/PD-L2 double positive cells following HMPV (Fig. 2B-C). While there were fewer total numbers of PD-L2^{+} cells in both groups, mock-infected neonates had a modestly increased number of PD-L2^{+} CD45^{+} leukocytes (Fig. 2C). Similar induction of PD-L1 on CD45^{-} non-immune cells was noted in neonatal and adult mice post-infection (Fig. S5B).

Several innate immune cell types had differences in PD-L1 and PD-L2 expression. There was a significant loss in total cell number and number of PD-L1^{+} alveolar macrophages (AMs) in the HMPV-infected adult group, while neonatal AMs had sustained PD-L1^{+} expression (Fig. 2E, S1C). Both uninfected and HMPV-infected neonates had increased PD-L1^{+}PD-L2^{+} AMs compared to adult counterparts (Fig. 2E, S5C). Both neonates and adults had increased total and PD-L1^{+} CD103^{+} dendritic cell (DC) populations after infection, while neonates at baseline had increased PD-L2^{+} and PD-L1^{+}PD-L2^{+} populations (Fig. 2E, S5C-D). Eosinophils in infected neonates had increased total, PD-L1^{+}, PD-L2^{+}, and PD-L1^{+}PD-L2^{+} populations when compared to infected adults (Fig. 2E, S5C-D). Neutrophils, interstitial macrophages (IMs), and monocytes showed similar numbers of PD-L1 and PD-L2 expression in infected neonates and adults (Fig. 2E, S5C-D). Several innate cells including AMs, CD103^{+} DCs, and neutrophils had sustained PD-L1 expression in HMPV-infected over the course of neonatal infection (Fig. S5E). Collectively, these data demonstrate that neonatal mice have evidence of increased PD-L1/PD-L2^{+} cell numbers (AMs, DCs) at baseline and can abundantly upregulate PD-L1/PD-L2 in various innate immune cells comparably to adult mice.

1.2.3. Neonatal CD8^{+} T cells upregulate PD-1 comparably to adult mice, but have reduced LAG3 expression

Given the swift upregulation of PD-1 ligands following HMPV infection and prior studies examining inhibitory receptors on adult CD8^{+} T cells [24,25,28], we next sought to characterize PD-1 expression on neonatal CD8^{+} T cells following HMPV. The preponderance of PD-1^{+} cells in both neonates and adults were CD8^{+} T cells, furthering our rationale for focusing on this population (Fig. S6). At day 7 post-infection, HMPV-infected B6 neonates demonstrated recruitment of CD8^{+} T cells to a similar degree as adult mice (Fig. 3A). Likewise, neonatal mice lacking the inhibitory receptor PD-1 (*Pdcd1*$^{-/-}$) had an influx of CD8^{+} T cells comparable in number to adult *Pdcd1*$^{-/-}$ mice (Fig. 3A). Both B6 and *Pdcd1*$^{-/-}$ neonates showed reduced percentages of effector CD8^{+} T cells (CD44^{+}CD62L^{-}) compared to adults following HMPV infection, though only the B6 neonates reached statistical significance compared to their adult counterparts (Fig. 3B-C). Neonates of both genotypes had an expanded CD44^{+}CD62L^{+} compartment compared to adult mice (Fig 3B-C). Neonatal B6 mice generated an HMPV-specific response similar in total cell number and frequency compared to adult B6 mice, as measured by an MHC class I tetramer containing the previously identified immunodominant M94 epitope from HMPV (Fig. 3D). Likewise, *Pdcd1*$^{-/-}$ neonates and adult mice generated a similar frequency and number of tetramer-positive cells. Consistent with a cytotoxic type 1 (Tc1) response [29], tetramer positive cells from all groups had marked upregulation of Tbet (Fig. S7). Tetramer-positive cells from both B6 adults and neonates had ubiquitous PD-1 expression, which was undetectable in

the *Pdcd1*$^{-/-}$ groups as expected (Fig. 3E). TIM3 was comparably upregulated in all groups, independent of genotype or age (Fig. 3F). Interestingly, the percent of LAG3-expressing cells was significantly increased in adult B6 compared to neonatal B6, with a similar trend noted in the *Pdcd1*$^{-/-}$ adults and neonates, though LAG3 MFI was similar in all groups (Fig. 3G). 2B4 had minimal expression on tetramer-positive cells from all groups, although B6 mice had an increase in 2B4 MFI (Fig. 3H).

Boolean gating analyses on M94^{+} cells for PD-1, TIM3, LAG3, and 2B4 demonstrated that fewer tetramer-positive cells isolated from HMPV-infected neonates co-expressed 2 or 3 inhibitory receptors when compared to adult M94^{+} cells (Fig. 3I). Similar analysis on *Pdcd1*$^{-/-}$ and B6 mice excluding PD-1^{+} M94^{+} cells from both B6 and *Pdcd1*$^{-/-}$ neonates showed similar expression patterns of TIM3, LAG3, and 2B4 (Fig. 3J). Thus, neonatal CD8^{+} T cells had reduced upregulation of surface markers of activation, similar expression of PD-1, but had a smaller proportion of cells with multiple inhibitory receptors expressed.

1.2.4. PD-1 inhibits canonical CD8^{+} T cell effector function in neonatal cells

CD8^{+} T cell effector functions were evaluated at day 7 post-infection by *ex vivo* peptide stimulation from mock-infected and HMPV-infected B6 neonates, B6 adults, *Pdcd1*$^{-/-}$ neonates, and *Pdcd1*$^{-/-}$ adults (Fig. 4). HMPV-infected mice from both B6 and *Pdcd1*$^{-/-}$ adults and neonates demonstrated comparable degrees of degranulation, as measured by percent positive for surface CD107a (Fig.4A). However, neonatal cells from both mock-infected mice of genotypes had a trend of increased CD107 MFI compared to adult mice (Fig. 4A).

Adult HMPV-infected B6 animals demonstrated increased granzyme B compared to age-matched mock-infected controls and neonatal HMPV-infected animals (Fig. 4B). Neonatal *Pdcd1*$^{-/-}$ CD8^{+} T cells had significantly increased granzyme B production compared to littermate mock-infected controls and B6-infected neonates (Fig. 4B). Neonatal *Pdcd1*$^{-/-}$ CD8^{+} T cells also had significantly increased IL-2 production compared to adult *Pdcd1*$^{-/-}$ CD8^{+} T cells and neonatal B6 CD8^{+} T cells (Fig. 4C). IFN-γ was significantly increased following infection in both B6 neonates and adults, but *Pdcd1*$^{-/-}$ neonates had a more robust IFN-γ response when compared to B6 neonates (Fig. 4D). Finally, perforin production by CD8^{+} T cells was significantly increased in HMPV-infected B6 adult mice and *Pdcd1*$^{-/-}$ adults and neonates (Fig. 4E).

To test whether this was specific to HMPV, we used a similar neonatal infection model with PR8 influenza. B6 neonatal mice infected with influenza had similar CD107a degranulation, reduced granzyme B, and reduced IL-2 production compared to B6 adult mice infected with influenza (Fig. S8A-C). However, neonatal CD8^{+} T cells infected with influenza had similar percentages of IFN-γ and perforin producing cells compared to adult mice (Fig. S5D-E). Therefore, decreased production of granzyme B and IL-2 by neonatal CD8^{+} T cells appears to be conserved independent of viral pathogen.

Interestingly, B6 neonatal CD8^{+} T cells degranulated but lacked classical effector functions. Previous studies have demonstrated that neonatal CD8^{+} T cells can generate reactive oxygen species (ROS) at baseline in the absence of infection.[30] Measurement of *ex vivo* ROS

production demonstrated that neonatal B6 $CD8^+$ T cells produced more ROS regardless of infection status compared to adult $CD8^+$ T cells (Fig. S9). Collectively, these data demonstrate that PD-1 acts to restrain classic $CD8^+$ T cell function in neonates while highlighting an effector mechanism unique to neonates.

1.2.5. PD-1 limits immunopathology following respiratory viral infection

Pdcd1$^{-/-}$ neonatal mice had similar kinetics of HMPV clearance compared to B6 mice, reaching the limit of detection by day 8 post-infection (Fig. 5A). However, *Pdcd1*$^{-/-}$ neonates demonstrated prominent immunopathologic features such as alveolar inflammation and large perivascular lymphoid aggregates at day 7 post-infection compared to B6 neonates, B6 adults, and *Pdcd1*$^{-/-}$ adults (Fig. 5B). *Pdcd1*$^{-/-}$ neonates had greater numbers of lymphocytic clusters compared to B6 neonates (Fig. 5C) and greater cluster size compared to *Pdcd1*$^{-/-}$ adults (Fig. 5D). To test whether this enhanced pathology in *Pdcd1*$^{-/-}$ neonates was HMPV-specific or a general response following acute respiratory viral infection, we used a lethal model of PR8 influenza [24]. *Pdcd1*$^{-/-}$ mice were shown previously to have reduced weight loss following influenza infection with strains of X31 influenza.[24,31] Similarly, we found at day 7 post-infection, *Pdcd1*$^{-/-}$ adult mice had modestly reduced weight loss in comparison to B6 adult mice (Fig 5E). However, using an LD_{50} of 250 PFU PR8, *Pdcd1*$^{-/-}$ neonates had significantly increased mortality compared to B6 neonates following PR8 challenge (Fig. 5F).

We next assessed for residual changes in lung inflammation and physiology in B6 and *Pdcd1*$^{-/-}$ mice 35 days after either primary HMPV infection as a neonate or as an adult. This timepoint was selected to allow for sufficient growth of the neonatal mice into nearly 6-week-old adult mice, thus allowing for the completion of postnatal alveolarization and for the evaluation of lung physiology in mice of similar sizes. Viral burden was undetectable in all groups at this time point. Compared to B6 mice infected as neonates, neonatal HMPV-infected *Pdcd1*$^{-/-}$ mice showed persistent lymphocytic infiltrates on day 35 post-infection, while small and scarce lymphoid aggregates were noted in the remaining groups (Figs. 6A-B). Additionally, *Pdcd1*$^{-/-}$ mice infected as neonates showed markedly abnormal alveolar architecture compared to B6 mice infected as neonates (Fig. 6A). As a measure of alveolar structure, septal volume density (Vv_{sep}) and mean linear intercept was quantified. *Pdcd1*$^{-/-}$ mice infected as neonates had significantly reduced septal volume density and significantly longer mean linear intercept distance compared to B6 neonates and *Pdcd1*$^{-/-}$ adult mice (Figs. 6C-D).

Functional airway testing using flexiVent showed *Pdcd1*$^{-/-}$ mice following neonatal infection showed evidence of increased quasi-static lung compliance and a reciprocal decrease in elastance (Fig. 6E), consistent with non-infectious models of neonatal lung injury.[32-34] In contrast, B6 mice following neonatal or adult infection, as well as *Pdcd1*$^{-/-}$ mice following adult infection, showed no significant changes in either measurement (Fig. 6E). Additionally, the tissue-related parameters of tissue elastance and tissue damping (ΔH and ΔG, respectively), were also decreased in *Pdcd1*$^{-/-}$ mice following neonatal infection, further suggestive of persistent alveolar damage following neonatal respiratory viral infection (Fig. 6F). Interestingly, these changes were not observed in B6 mice at

either age or *Pdcd1*$^{-/-}$ adult mice following infection (Fig. 6F). Two different measures of resistance (Rrs, Rn) were significantly reduced in *Pdcd1*$^{-/-}$ mice infected as neonates compared to *Pdcd1*$^{-/-}$ adult mice, further suggesting abnormal changes to lung physiology (Fig. 6G).

Pdcd1$^{-/-}$ mice infected with HMPV as neonates had several features consistent with an activated CD8^{+} T cell response at day 35 post-infection. First, *Pdcd1*$^{-/-}$ mice infected as neonates had an increased total number of CD8^{+} T cells in the lung compared to mock-infected littermate controls (Fig. 6H). These data were supported by immunohistochemical staining of the lungs, which showed *Pdcd1*$^{-/-}$ mice infected as neonates had a robust CD8^{+} population in the lungs, including within the lymphoid structures (Fig. S10A). In contrast, B6 but not *Pdcd1*$^{-/-}$ mice infected with HMPV as neonates had increased CD4^{+} T cell and CD19^{+} B cell numbers in the lungs 35 days after infection (Fig. S10B). All infected groups showed similar M94-tetramer positive cell number and frequency, suggesting the virus-specific response contracted equally among the genotypes (Fig. 6I, S10C). *Pdcd1*$^{-/-}$ mice infected as neonates had a statistically significant increased proportion of activated CD44^{+}CD62L^{+} CD8^{+} T cells compared to B6 neonates, while a similar trend was noted between adult groups (Fig. S10D).

Consistent with persistent CD8^{+} T cell activation, there was an increased granzyme B protein on day 35 post-infection in the lung homogenate of *Pdcd1*$^{-/-}$ mice infected with HMPV as neonates (Fig. 6J). Likewise, the percent of granzyme B-expressing CD8^{+} T cells were significantly increased in the *Pdcd1*$^{-/-}$ mice infected as neonates compared to adult infected *Pdcd1*$^{-/-}$ mice (Fig. S10E). but not B6 mice infected as neonates or *Pdcd1*$^{-/-}$ adults. Similarly, while B6 mice infected as neonates showed minimal IL-2 production compared to B6 mice infected as adults, *Pdcd1*$^{-/-}$ mice infected as neonates showed a trend towards increased IL-2 production (Fig. S10F). IFN-γ positive cells were comparable across groups (Fig. S10G). Analyses of several other cytokines by Luminex, including IL-2 and IFN-γ, showed similar protein quantity between neonatal mice mock-infected and HMPV-infected B6 and *Pdcd1*$^{-/-}$ at day 35 post-infection (Fig. S11). Collectively, these data demonstrate *Pdcd1*$^{-/-}$ mice infected as neonates have markedly abnormal lung function with evidence of a persistent aberrant CD8^{+} T cell response 35 days following HMPV infection.

1.2.6. Evidence of increased effector function in CD8^{+} T cells from a child without PD-1 signaling

To test whether these findings were reflected in human immunopathology, we queried a previously published single cell RNA sequencing dataset from a case of a young child with a homozygous frameshift mutation in the *PDCD1* gene.[35] This patient had severe multi-organ autoimmunity, severe tuberculosis caused by *Mycobacterium tuberculosis*, and fatal alveolar hemorrhage secondary to presumed pulmonary autoimmunity at 11 years.[35] Following integration of single cell RNA sequencing data from the patient, his healthy sibling, and 5 pediatric and adult controls, several adaptive immune cell clusters were identified (Fig. S12A), including several CD8^{+} T cell subsets. B cells and monocytes could also be identified (Fig. S12B). Evaluating the relative abundance of each cell type, the PD-1 deficient child had evidence of increased activated cells (characterized by high levels of

Ki67, a division marker, and IFN signature genes) (Fig. S12C). As previously reported, the PD-1 deficient patient had reduced V$\delta2^+$ $\gamma\delta$ T cells [35] Evaluation of effector molecules such as granzymes and perforin was performed on individual cell clusters. $CD8^+$ central memory T cells, double-negative T cells, Th1, and Th1* cells all demonstrated enhanced granzyme B expression in the PD-1 deficient patient when compared to pediatric healthy controls, which had low levels of granzyme B at baseline (Fig. S12D). V$\delta2^+$ $\gamma\delta$ T cells had high levels of granzyme B in healthy children, which was further enhanced in the PD-1-deficient patient (Fig. S12D). $CD8^+$ effector cells, $CD8^+$ TEMRA, activated cells, NK cells, and plasmacytoid dendritic cells also had strong granzyme B signatures, which again were enhanced in the PD-1-deficient patient (Fig. S12D). Interestingly, other granzymes (GzmA, GzmH, GzmK, and GzmM) and perforin transcripts were not specifically enhanced in the $CD8^+$ central memory or V$\delta2^+$ $\gamma\delta$ T cells from this patient, suggesting unique alterations in granzyme B transcriptional regulation in the absence of PD-1 in $CD8^+$ T cells. Further corroborating these findings, T-cell blasts from the PD-1-deficient patient had a trend towards increased granzyme B production following stimulation with anti-CD3 and anti-CD3/CD28 stimulation conditions when compared his sibling with intact PD-1 signaling (Fig. S12E).

Collectively, these results indicate that an increased T cell activation signature and the expression of granzyme B was observed in a child with PD-1 deficiency and fatal lung immunopathology, consistent with the phenotypes seen in young *Pdcd1*$^{-/-}$ mice with respiratory viral infection.

1.3. Discussion

In the context of an acute respiratory viral infection, the neonatal lung must strike a delicate balance between mounting a protective antiviral response while mitigating damage to the development process. Here, we demonstrate that while neonatal mice are capable of mounting an antigen-specific $CD8^+$ T cell response following HMPV infection similar to adult mice, there are several differences that highlight the importance of PD-1 mediated inhibition of neonatal $CD8^+$ cells (Table 1).[25] First, there are increased PD-$L1^+$ and PD-$L1^+$PD-$L2^+$ innate populations at baseline and following infection in the neonatal lung. Second, neonatal $CD8^+$ T cells had similar induction of PD-1 but had fewer cells with multiple inhibitory receptor expression driven largely by decreased LAG3 expression. LAG3 is an important inhibitory receptor shown previously to work in conjunction with PD-1 to limit effector function during respiratory viral infection [25], suggesting neonatal CD8s may have reduced redundancy of inhibitory receptors (Table 1). Third, while neonatal $CD8^+$ T cells had reduced production of several key effector cytokines associated with adult $CD8^+$ T cells, such as granzyme B, IFN-γ, and IL-2 following HMPV infection, these functions are robustly restored in the absence of PD-1 (Table 1). Lastly, rather than the beneficial effect of PD-1 disruption shown previously in adult murine respiratory virus models, lack of PD-1 signaling during neonatal viral infection leads to both acute and chronic immunopathology in the lung (Table 1).

Neonates and infants were once thought to be in a state of relative immunosuppression, with a disorganized and limited adaptive immune response.[36-39] However, recent studies

suggest a more nuanced layered state of adaptive immunity in neonates, where similar cell types (e.g. $CD8^+$ T cells) arising at different points in life have disparate functions.[39-42] For example, when adoptively transferred into an adult mouse and challenged with a systemic viral infection, neonatal $CD8^+$ T cells were shown to rapidly proliferate and quickly assume a terminally differentiated state at the expense of long-term memory formation.[43] Further work 'timestamping' the effector $CD8^+$ T cell compartment in developing mice showed that neonatal $CD8^+$ T cells continue to have an altered epigenetic landscape and rapid effector responses into adulthood.[44] Human naïve $CD8^+$ T cells isolated from peripheral blood of neonates and adults showed different transcriptional and epigenetic profiles, with neonatal $CD8^+$ T cells showing enhanced proliferation, increased 'innate-like' properties like production of reactive oxygen species, and decreased cytotoxic effector production, such as granzyme B and IFN-γ.[30]

Following HMPV infection during the first week of life, we found that murine neonatal $CD8^+$ T cells similarly demonstrated reduced granzyme B production compared to adult $CD8^+$ T cells. Likewise, in a neonatal RSV model, neonatal $CD8^+$ T cells showed a diminished IFN-γ response compared to adult cells.[45] Furthermore, that blunted IFN-γ response following neonatal RSV could be rescued with use of inhaled recombinant IFN-γ, an intervention that led to reduced weight loss, enhanced viral clearance, and improved macrophage function.[27] In both human and murine samples, neonatal DCs demonstrated diminished co-stimulatory receptor expression due to poor responsiveness to type I IFN, suggesting that blunted neonatal APC responses are a contributing factor to poor $CD8^+$ T cell function.[13] We found in the current work that $CD8^+$ T cells were not incapable of producing granzyme B or IFN-γ due to differences in the immunologic milieu of the neonatal lung or intrinsic cellular differences, but rather were actively constrained by PD-1 signaling, indicating that multiple levels of neonatal immune control likely exist. Despite the increased production of cytotoxic effectors, though, *Pdcd1*$^{-/-}$ neonates had similar kinetics of viral clearance. These data suggest that cell types other than $CD8^+$ T cells or humoral mediators contribute to viral clearance in the neonatal lung.

Interestingly, both neonatal and adult $CD8^+$ T cells demonstrated similar levels of surface CD107, consistent with degranulation, following HMPV infection. In B6 neonatal mice, however, degranulation occurred in the absence of typical effector functions, such as granzyme B production. Neonatal $CD8^+$ T cells produced reactive oxygen species (ROS), a previously identified unique effector function to neonatal cells [30], in both the presence and absence of HMPV. Therefore, it is possible that neonatal $CD8^+$ T cells have an increase in degranulation under homeostatic and HMPV-infected conditions consistent with ROS production and release. Additionally, neonatal $CD8^+$ T cells showed reduced granzyme B and IL-2 production following influenza infection; these data support the notion that neonatal CD8s have fewer classical effector functions compared to adult $CD8^+$ T cells in the context of various viral infections.

Inhibition of $CD8^+$ T cells following respiratory viral infection has been described by our group and others.[22,24,26,31] Increased expression of inhibitory receptors, particularly PD-1 and LAG3, leads to impairment of $CD8^+$ function with reduced degranulation, IFN-γ production, and granzyme B production following viral challenge.[24,25] Blockade of PD-1

ligands led to a more robust antigen-specific $CD8^+$ T cell response and reduced viral titer in the lungs.[24] From a pathologic perspective, there was a self-resolving increase in breath distention following anti-PD-L1/2 blockade, while disruption of PD-1 alone showed no evidence of increased inflammation.[24] However, we found that neonates—perhaps in part due to decreased LAG3 upregulation—appear to have a diminished capacity to tolerate PD-1 disruption following HMPV infection, as *Pdcd1*$^{-/-}$ pups showed marked acute histopathologic changes. Furthermore, constraint of an exuberant antiviral response in the neonatal period also mitigated longstanding pathologic effects, as evidenced by changes in compliance/elastance specifically in *Pdcd1*$^{-/-}$ neonates mice 35 days following HMPV infection. Evidence of $CD8^+$ activation, including IL-2 production and protein levels of granzyme B, were still detectable in the *Pdcd1*$^{-/-}$ mice infected as neonates at 35 days post-infection. Moreover, at this late time point, *Pdcd1*$^{-/-}$ mice infected as neonates had evidence of alveolar simplification with an increased mean linear intercept and decreased septal volume density. Alveolar simplification has been described in models of bronchopulmonary dysplasia, whereby abnormal lung development occurs secondary to an injury or insult in early life.[46] The persistent inflammatory signature and chronic histopathology suggest that the developing lung is unable to tolerate a global loss of PD-1 signaling when faced with a respiratory viral infection.

Disruption of PD-1 signaling in other clinical contexts emphasizes the importance of this pathway, particularly in the lung. First, a common adverse effect of checkpoint inhibitors targeting PD-1 in patients with malignancy is immune-mediated pneumonitis, which has an estimated incidence of 3-5%.[47-49] The outcomes of PD-1 blockade-associated pneumonitis can range from resolution with a drug holiday, to response to immunosuppression, to death (1% of cases in a phase I trial).[48,49] Additionally, two siblings with PD-1 deficiency, one suspected and one experimentally confirmed, both died of pneumonitis of suspected autoimmune etiology by age 11 years, further evidencing the indispensable role of PD-1 in preventing pulmonary immunopathology in children. Consistent with the data in neonatal *Pdcd1*$^{-/-}$ mice, we show that multiple types of T cells, including central memory $CD8^+$ T cells, of the PD-1-deficient child had an elevated expression of granzyme B compared to healthy age-matched controls. Granzyme B is a serine protease with multiple intracellular and extracellular functions, including induction of apoptosis, cleavage of extracellular matrix components, processing of cytokines such as IL-1, etc.[50] Elevated granzyme B in a developing lung undergoing postnatal alveolarization could be quite damaging given the wide range of inflammatory functions above. However, granzyme B may not be the primary causal factor in the chronic lung changes seen following HMPV infection, but rather a surrogate marker of unresolved inflammation from a neonatal infection in the absence of PD-1. Regardless, the combination of the striking lung changes in neonatal *Pdcd1*$^{-/-}$ mice following respiratory viral infection and the devastating pulmonary manifestations in PD-1-deficient children further highlights the indispensable role of PD-1 in limiting immunopathology in the lung in the childhood.

Future studies could evaluate neonates and children with severe respiratory viral infection for evidence of PD-1-related dysregulation. In a murine model, understanding the relationship between specific cytotoxic $CD8^+$ T cell function, and the outcomes on lung development can be investigated mechanistically. Moreover, though restoration of $CD8^+$

T cell effector function occurred in the absence of PD-1, viral burden was unchanged. Additional studies comparing the intrinsic differences between neonatal and adult $CD8^+$ T cells following HMPV infection with/without PD-1 signaling, including evaluating the epigenetic landscape, assessing for atypical effector molecules, and mechanisms of differential LAG3 upregulation could identify other mediators. The role of PD-1 signaling on other cell types, including $CD4^+$ T cells, should also be explored in the context of neonatal murine HMPV infection. However, PD-1-dependent inhibition of neonatal $CD8^+$ T cells during respiratory virus infection supports the hypothesis that the immune response in neonates is not deficient simply due to immaturity, but rather is specifically regulated to limit damage in the unique milieu of the developing lung.

1.4. Materials and Methods

Mice and virus stocks

C57BL/6 mice (strain: 000664) and *Rag1*$^{-/-}$ mice (strain: 034159) were purchased from The Jackson Laboratory. *Pdcd1*$^{-/-}$ mice were obtained with permission from Tasuku Honjo (Kyoto University, Kyoto, Japan) and kindly shared by Karen Haas (Wake Forest University). Breeder pairs were set up with 6-8-week-old mice of each strain and monitored daily for signs of pregnancy. Breeder pairs were used for 6 months or until cessation of reproduction. Following delivery of pups, neonatal mice were anesthetized with 3% isoflurane in a heated chamber and infected intranasally with $2.8x10^6$ PFU of HMPV strain TN/94-49 (genotype A2) in 10μL sterile PBS at day 4-6 of life. Six-to-eight-week adult mice were infected with $2.8x10^6$ PFU HMPV in 100μL sterile PBS via orotracheal inoculation. TN/94-49 was grown in LLC-MK2 cells and purified as previously described.[51] Influenza virus strain A/34/PR/8 (H1N1) was obtained from ATCC, grown in MDCK cells, and titered on LLC-MK2 cells as previously described.[24] A mock lysate was prepared using the same protocol with uninfected LLC-MK2 cells; an equal volume of mock lysate was administered to animals as HMPV or PR8 inoculum. Littermates were randomized to either receive virus or mock lysate. Neonatal mice were euthanized via isoflurane anesthesia and decapitation, while adult mice were euthanized using CO_2 asphyxiation. Each experiment was performed on two separate litters. All protocols were approved by the University of Pittsburgh IACUC.

Viral burden titration

Viral titers were measured via plaque titration.[51,52] Briefly, a monolayer of LLC-MK2 cells grown in a 24-well tissue culture dish was washed twice with sterile PBS. Lung homogenates were serially diluted 1:10 in 0% Opti-MEM media containing 1:2000 trypsin and added to the plate in triplicate, followed by one-hour rocking incubation at room temperature. Overlay media containing 0.75% methylcellulose and 1:500 trypsin was added and plates were incubated at 37°C for 5 days. Plates were fixed with 10% formalin, blocked with PBST containing 5% milk, and stained using 1:1000 guinea pig anti-HMPV primary antibody and 1:1000 anti-guinea pig-HRP secondary antibody. Plates were developed using TrueBlue™ substrate (KPL, Cat:5510-0050) and quantified.

Histology

Following dissection and isolation, the left lung lobe was insufflated with 10% formalin, embedded in paraffin, sectioned, and stained with H&E. CD8 immunohistochemistry (IHC) staining was performed by the CHP pathology core, using recombinant anti-CD8 alpha antibody (Abcam, Cat: ab217344, clone: EPR21769). Images for each figure were captured and processed using Adobe Photoshop using the same parameters per figure. Measurement of alveolar septal wall thickness was performed using ImageJ 1.54g. The average of 10 measurements per high-powered field of alveolar septal wall thickness was calculated. Lymphocytic clusters were manually counted and diameter was measured via SPOT imaging software (v4.6). Septal volume density (Vv_{sep}) and mean linear intercept (Lm) were calculated using the semi-automated morphometry plugin for FIJI (morphometry v.4.0) by evaluating five representative images per animal.[53]

Protein quantification

Lung homogenates were clarified by centrifugation and analyzed via ProcartaPlex™ Mix & Match panels (Invitrogen, Cat:PPX-18-MX47XXDD) per manufacturer's instructions. Analytes included: PD-L1, PD-L2, Eotaxin (CCL11), IFN alpha, IFN beta, IFN gamma, IL-2, IL-4, IL-5, IL-10, IL-13, IL-15, IL-17A (CTLA-8), IL-22, IL-23, IL-33, IP-10 (CXCL10), MIG (CXCL9). Granzyme B was measured using a commercially available ELISA per manufacturer's instruction (Thermo, Cat: BMS6029).

Flow cytometry

Lung tissue was harvested, minced with scissors, and subjected to one-hour digestion via collagenase/DNase at 37°C. Following digestion, lung tissue was passed through a 70μm strainer, treated with RBC lysis buffer (ACK, Gibco, Cat:A1049210) for 1 minute, followed by resuspension in RPMI+10%FBS. For T cell characterization, cells were then plated for *ex vivo* peptide stimulation or tetramer staining in parallel. For peptide stimulation, cells were stimulated with 10μM M94, NP366, or irrelevant control peptide in the presence of BFA/monensin and CD107-PE antibody for 5 hours at 37°C as described previously.[54,55] Control stimulation conditions included unstimulated cells and cells treated with PMA/ionomycin. Cells were then washed, stained with live/dead violet (1:1000 in PBS, Invitrogen, Cat:L34964A) for 15 minutes, washed x2 in PBS, incubated with anti-CD16/CD32 (1:100 in FACS buffer, Tonbo™, Cat:70-0161-M001) for 20 minutes, and then stained for surface markers (1.5μL antibody/sample in BD Horizon™ Buffer, Cat:566349) for 40mins at 4°C (Supplemental Table 1). Cells were then washed x2 in FACS, fixed with Foxp3 fix/permeabilization buffer (Invitrogen, Cat:50-112-8857) for 20 mins at 4°C, followed by intracellular staining (4.5μL antibody/sample in 1:1 mixture of BD buffer and fix/perm buffer) for 30 minutes at 4°C (Supplemental Table 1). Cells were then washed in fix/perm buffer x2 and resuspended in FACS buffer. Peptide plate gating strategy can be found in Fig. S1.

For tetramer staining, cells were incubated for 30mins at RT in FACS buffer containing dasatinib, followed by 1:100 M94 class I tetramer or an irrelevant tetramer for 90 minutes at RT in the dark. Cells were then washed and incubated with live/dead, anti-CD16/CD32, and surface stain and inhibitory receptors as described above (Supplemental Table 1). Following

wash with FACS buffer, cells were fixed with FoxP3 fix/perm for 18hours at 4°C. Cells were then washed x1 in fix/perm buffer and stained for transcription factors (2.5μL antibody/sample in 1:1 mixture of BD buffer and fix/perm buffer) for 1 hour at 4°C (Supplemental Table 1). Cells were then washed in fix/perm buffer x2 and resuspended in FACS buffer and 100μL of Biolegend Counting Beads were added. Fluorescence minus one (FMO) controls were used for all inhibitory receptors and isotype control used with Tbet as shown in the gating strategy (Fig. S2).

For innate cell marker and PD-L1 staining, a single cell suspension was generated followed by live/dead staining, anti-CD16/CD32 blockade, and surface stains as above (Supplemental Table 1). Cells were then fixed in 2% PFA for 20 minutes and subsequently resuspended in FACS buffer. Gating strategy was adapted from Misharin *et al* (Fig. S3).[56]

For all conditions, samples were strained through nylon filters and run on a Cytek® Aurora multispectral flow cytometer. Unstained cells from each experiment were generated using 2% PFA and used to minimize autofluorescence. Data analysis was performed with Flowjo(v10.8.1).

Ex vivo reactive oxygen species (ROS) measurement

ROS measurement was performed as previously described.[57] A single cell suspension from lung cells was generated as above. For each individual sample, 50μL of cells were plated, followed by Fc block 1:100 for 15 minutes at room temperature. CD19, CD3, CD8, CD4, CD44, and CD62L antibodies were added (1.5μL/sample in 50μL of FACS) with a 20-minute incubation. MitoSOX Red (ThermoFisher Cat:M36008) was resuspended in DMSO and diluted 1:100 in FACs buffer. After the surface antibody incubation, 5μL of diluted MitoSOX was added per well with a 20-minute incubation at 37°C. Following incubation, cells were washed twice with FACS buffer and immediately run on a Cytek® Aurora. An unstained control and no MitoSOX control were analyzed with each experiment. Gating strategy was similar to peptide gating with measurement of ROS on PE channel.

Lung physiology parameter measurement

Thirty-five days following a neonatal infection, mice were anesthetized with pentobarbital (90mg/kg) via intraperitoneal injection and the trachea was then exposed, cannulated, and connected to a computer-controlled small-animal mechanical ventilator (flexiVent; SCIREQ, Montreal, QC, Canada). Pulmonary function was assessed as previously described [58]. First, the quasi-static mechanical properties of the lung at baseline (compliance) were measured using pressure-volume curves (stepwise pressure-driven perturbation). Next, respiratory system mechanics at baseline were assessed by collecting three consecutive measurements using the single frequency forced oscillation technique followed by three consecutive measurements using the broadband frequency forced oscillation technique. Using the single frequency force oscillation maneuver, total respiratory system resistance (Rrs) and elastance (Ers) were reported as the average of the three measurements. Airway resistance (Rn) and tissue-related parameters (G, tissue damping and H, tissue elastance) were calculated using the constant phase model as previously described[59], and the average of each parameter was reported.

Single cell RNA sequencing analyses

Peripheral blood mononuclear cells (PBMCs) were isolated from the index patient lacking with a homozygous frameshift in *PDCD1*, a healthy 6-year old sibling, 5 healthy pediatric controls, and 5 healthy adult controls as previously described.[35] Following integration of the datasets, relative abundance of several adaptive immune cells could be evaluated. Clustering and cell type annotation was performed as previously described.[60] To evaluate gene expression, cells in a given cluster from a given sample were aggregated using the 'pseudobulk' method.[61] Log_2 fold change of specific genes was then estimated using DESeq2 with batch correction. To identify cells with high levels of transcripts of genes associated with CD8 effector function, normMean was calculated with average pseudobulk read counts using the healthy pediatric controls with further normalization based on housekeeping genes.

Human T cell stimulation assay

Thawed T-cells from a PD-1-deficient patient, his sibling with intact PD-1 signaling, and his father with heterozygous inheritance of PD-1 mutation were plated and stimulated with a variety of conditions for 24 hours.[35,62] Specific conditions included: media alone, anti-CD3 beads, Dynabeads Human T-Activator CD3/CD28, anti CD2/CD3/CD28 beads, PHA, or PMA/ionomycin, as previously described.[35,62] Cell supernatants were then collected and analyzed via LEGENDplex.

Statistics

All data displayed as mean±SEM. All statistical analysis was performed using GraphPad Prism (v.9.3.0). Weight curves were analyzed using simple linear regression comparing the rate of weight gain (e.g., slope) between groups. Analyses with two groups were analyzed using Mann-Whitney tests, while analyses with three or more groups were analyzed using a Kruskal-Wallis test. Multiple Mann-Whitney tests were used to analyze studies in which mock vs. HMPV-infected animals were compared between mice of differing genotypes/ages. Kruskal-Wallis tests were utilized for comparing mice of similar infection status across groups. For $CD44^+/CD62L^+$ analysis, a two-way ANOVA with multiple comparisons was utilized. All figures are the combination of studies performed at least two independent times. Kaplan-Meier survival analysis was performed for survival studies. Significance was defined as $p<0.05$ for all analyses.

Supplementary Material

Refer to Web version on PubMed Central for supplementary material.

Acknowledgments

Supported by NIHAI085062 (JVW), T32GM-008208 (OBP), T32AI089443 (YZ), and the Henry L. Hillman Foundation (JVW). Research reported in this publication was supported by the Eunice Kennedy Shriver National Institute of Child Health & Human Development of the National Institutes of Health under Award Number K12HD000850 (TE). The content is solely the responsibility of the authors and does not necessarily represent the official views of the National Institutes of Health. We thank the University of Pittsburgh Unified Flow Core and Children's Hospital of Pittsburgh Histology Core for help with this work. We thank the NIH Tetramer Core Facility (contract number 75N93020D00005) for providing tetramers.

LITERATURE CITED

1. Perin J. et al. Global, regional, and national causes of under-5 mortality in 2000-19: an updated systematic analysis with implications for the Sustainable Development Goals. Lancet Child Adolesc. Health 6, 106–115 (2022). [PubMed: 34800370]
2. Wang X. et al. Global burden of acute lower respiratory infection associated with human metapneumovirus in children under 5 years in 2018: a systematic review and modelling study. Lancet Glob. Health 9, e33–e43 (2021). [PubMed: 33248481]
3. Shi T. et al. Global, regional, and national disease burden estimates of acute lower respiratory infections due to respiratory syncytial virus in young children in 2015: a systematic review and modelling study. Lancet 390, 946–958 (2017). [PubMed: 28689664]
4. Wang X. et al. Global burden of respiratory infections associated with seasonal influenza in children under 5 years in 2018: a systematic review and modelling study. Lancet Glob. Health 8, e497–e510 (2020). [PubMed: 32087815]
5. Stein RT et al. Respiratory syncytial virus hospitalization and mortality: Systematic review and meta-analysis. Pediatr. Pulmonol 52, 556–569 (2017). [PubMed: 27740723]
6. Edwards KM et al. Burden of human metapneumovirus infection in young children. N. Engl. J. Med 368, 633–643 (2013). [PubMed: 23406028]
7. Maitre NL & Williams JV Human metapneumovirus in the preterm neonate: current perspectives. RRN 6, 41–49 (2016).
8. Arruda E. et al. The burden of single virus and viral coinfections on severe lower respiratory tract infections among preterm infants: a prospective birth cohort study in Brazil. Pediatr. Infect. Dis. J 33, 997–1003 (2014). [PubMed: 25361184]
9. García-Garcia ML et al. Clinical and virological characteristics of early and moderate preterm infants readmitted with viral respiratory infections. Pediatr. Infect. Dis. J 34, 693–699 (2015). [PubMed: 25923427]
10. Warburton D. et al. Lung organogenesis. Curr. Top. Dev. Biol 90, 73–158 (2010). [PubMed: 20691848]
11. Restori KH, Srinivasa BT, Ward BJ & Fixman ED Neonatal immunity, respiratory virus infections, and the development of asthma. Front. Immunol 9, 1249 (2018). [PubMed: 29915592]
12. Eddens T, Parks OB & Williams JV Neonatal immune responses to respiratory viruses. Front. Immunol 13, 863149 (2022). [PubMed: 35493465]
13. Lau-Kilby AW et al. Type I IFN ineffectively activates neonatal dendritic cells limiting respiratory antiviral T-cell responses. Mucosal Immunol. 13, 371–380 (2020). [PubMed: 31797910]
14. Chelvarajan RL et al. Defective macrophage function in neonates and its impact on unresponsiveness of neonates to polysaccharide antigens. J. Leukoc. Biol 75, 982–994 (2004). [PubMed: 14982942]
15. Langrish CL, Buddle JC, Thrasher AJ & Goldblatt D Neonatal dendritic cells are intrinsically biased against Th-1 immune responses. Clin. Exp. Immunol 128, 118–123 (2002). [PubMed: 11982599]
16. Aksoy E. et al. Interferon regulatory factor 3-dependent responses to lipopolysaccharide are selectively blunted in cord blood cells. Blood 109, 2887–2893 (2007). [PubMed: 17138826]
17. De Wit D. et al. Blood plasmacytoid dendritic cell responses to CpG oligodeoxynucleotides are impaired in human newborns. Blood 103, 1030–1032 (2004). [PubMed: 14504106]
18. Danis B. et al. Interferon regulatory factor 7-mediated responses are defective in cord blood plasmacytoid dendritic cells. Eur. J. Immunol 38, 507–517 (2008). [PubMed: 18200500]
19. Papaioannou NE et al. Environmental signals rather than layered ontogeny imprint the function of type 2 conventional dendritic cells in young and adult mice. Nat. Commun 12, 464 (2021). [PubMed: 33469015]
20. Cormier SA et al. Limited type I interferons and plasmacytoid dendritic cells during neonatal respiratory syncytial virus infection permit immunopathogenesis upon reinfection. J. Virol 88, 9350–9360 (2014). [PubMed: 24920801]

21. Gollwitzer ES et al. Lung microbiota promotes tolerance to allergens in neonates via PD-L1. Nat. Med 20, 642–647 (2014). [PubMed: 24813249]
22. Telcian AG et al. RSV-induced bronchial epithelial cell PD-L1 expression inhibits CD8+ T cell nonspecific antiviral activity. J. Infect. Dis 203, 85–94 (2011). [PubMed: 21148500]
23. McNally B, Ye F, Willette M & Flaño E Local blockade of epithelial PDL-1 in the airways enhances T cell function and viral clearance during influenza virus infection. J. Virol 87, 12916–12924 (2013). [PubMed: 24067957]
24. Erickson JJ et al. Viral acute lower respiratory infections impair CD8+ T cells through PD-1. J. Clin. Invest 122, 2967–2982 (2012). [PubMed: 22797302]
25. Erickson JJ, Rogers MC, Tollefson SJ, Boyd KL & Williams JV Multiple Inhibitory Pathways Contribute to Lung CD8+ T Cell Impairment and Protect against Immunopathology during Acute Viral Respiratory Infection. J. Immunol 197, 233–243 (2016). [PubMed: 27259857]
26. Yao S. et al. Control of pathogenic effector T-cell activities in situ by PD-L1 expression on respiratory inflammatory dendritic cells during respiratory syncytial virus infection. Mucosal Immunol. 8, 746–759 (2015). [PubMed: 25465101]
27. Empey KM et al. Stimulation of immature lung macrophages with intranasal interferon gamma in a novel neonatal mouse model of respiratory syncytial virus infection. PLoS ONE 7, e40499 (2012). [PubMed: 22792355]
28. Erickson JJ, Rogers MC, Hastings AK, Tollefson SJ & Williams JV Programmed death-1 impairs secondary effector lung $CD8^+$ T cells during respiratory virus reinfection. J. Immunol 193, 5108–5117 (2014). [PubMed: 25339663]
29. Zhu Y. et al. T-bet and eomesodermin are required for T cell-mediated antitumor immune responses. J. Immunol 185, 3174–3183 (2010). [PubMed: 20713880]
30. Galindo-Albarrán AO et al. CD8+ T Cells from Human Neonates Are Biased toward an Innate Immune Response. Cell Rep. 17, 2151–2160 (2016). [PubMed: 27851975]
31. Pauken KE et al. The PD-1 Pathway Regulates Development and Function of Memory CD8+ T Cells following Respiratory Viral Infection. Cell Rep. 31, 107827 (2020). [PubMed: 32610128]
32. Yee M. et al. Type II epithelial cells are critical target for hyperoxia-mediated impairment of postnatal lung development. Am. J. Physiol. Lung Cell. Mol. Physiol 291, L1101–11 (2006). [PubMed: 16861382]
33. Dauger S. et al. Neonatal exposure to 65% oxygen durably impairs lung architecture and breathing pattern in adult mice. Chest 123, 530–538 (2003). [PubMed: 12576377]
34. Yee M. et al. Neonatal oxygen adversely affects lung function in adult mice without altering surfactant composition or activity. Am. J. Physiol. Lung Cell. Mol. Physiol 297, L641–9 (2009). [PubMed: 19617311]
35. Ogishi M. et al. Inherited PD-1 deficiency underlies tuberculosis and autoimmunity in a child. Nat. Med 27, 1646–1654 (2021). [PubMed: 34183838]
36. Adkins B, Leclerc C & Marshall-Clarke S Neonatal adaptive immunity comes of age. Nat. Rev. Immunol 4, 553–564 (2004). [PubMed: 15229474]
37. Ridge JP, Fuchs EJ & Matzinger P Neonatal tolerance revisited: turning on newborn T cells with dendritic cells. Science 271, 1723–1726 (1996). [PubMed: 8596932]
38. Garcia AM, Fadel SA, Cao S & Sarzotti M T cell immunity in neonates. Immunol. Res 22, 177–190 (2000). [PubMed: 11339354]
39. Rudd BD Neonatal T cells: A reinterpretation. Annu. Rev. Immunol 38, 229–247 (2020). [PubMed: 31928469]
40. Herzenberg LA & Herzenberg LA Toward a layered immune system. Cell 59, 953–954 (1989). [PubMed: 2688900]
41. Adkins B. Peripheral CD4+ lymphocytes derived from fetal versus adult thymic precursors differ phenotypically and functionally. J. Immunol 171, 5157–5164 (2003). [PubMed: 14607915]
42. Wang J. et al. Fetal and adult progenitors give rise to unique populations of CD8+ T cells. Blood 128, 3073–3082 (2016). [PubMed: 28034872]
43. Smith NL et al. Rapid proliferation and differentiation impairs the development of memory CD8+ T cells in early life. J. Immunol 193, 177–184 (2014). [PubMed: 24850719]

44. Smith NL et al. Developmental Origin Governs CD8+ T Cell Fate Decisions during Infection. Cell 174, 117–130.e14 (2018). [PubMed: 29909981]
45. Tregoning JS, Yamaguchi Y, Harker J, Wang B & Openshaw PJM The role of T cells in the enhancement of respiratory syncytial virus infection severity during adult reinfection of neonatally sensitized mice. J. Virol 82, 4115–4124 (2008). [PubMed: 18272579]
46. Dylag AM, Haak J, Yee M & O'Reilly MA Pulmonary mechanics and structural lung development after neonatal hyperoxia in mice. Pediatr. Res 87, 1201–1210 (2020). [PubMed: 31835269]
47. Fillatre P. et al. Incidence of Pneumocystis jiroveci pneumonia among groups at risk in HIV-negative patients. Am. J. Med 127, 1242.e11–7 (2014).
48. Naidoo J. et al. Pneumonitis in Patients Treated With Anti-Programmed Death-1/Programmed Death Ligand 1 Therapy. J. Clin. Oncol 35, 709–717 (2017). [PubMed: 27646942]
49. Nishino M, Sholl LM, Hodi FS, Hatabu H & Ramaiya NH Anti-PD-1-Related Pneumonitis during Cancer Immunotherapy. N. Engl. J. Med 373, 288–290 (2015). [PubMed: 26176400]
50. Velotti F, Barchetta I, Cimini FA & Cavallo MG Granzyme B in Inflammatory Diseases: Apoptosis, Inflammation, Extracellular Matrix Remodeling, Epithelial-to-Mesenchymal Transition and Fibrosis. Front. Immunol 11, 587581 (2020). [PubMed: 33262766]
51. Williams JV, Tollefson SJ, Johnson JE & Crowe JE The cotton rat (Sigmodon hispidus) is a permissive small animal model of human metapneumovirus infection, pathogenesis, and protective immunity. J. Virol 79, 10944–10951 (2005). [PubMed: 16103146]
52. Xu J, Zhang Y & Williams JV Development and optimization of a direct plaque assay for trypsin-dependent human metapneumovirus strains. J. Virol. Methods 259, 1–9 (2018). [PubMed: 29807042]
53. Salaets T. et al. A semi-automated method for unbiased alveolar morphometry: Validation in a bronchopulmonary dysplasia model. PLoS ONE 15, e0239562 (2020). [PubMed: 32966330]
54. Eddens T. et al. Monocyte production of C1q potentiates CD8 + T cell effector function following respiratory viral infection. BioRxiv (2023).doi: 10.1101/2023.06.04.543430
55. Parks OB et al. Human Metapneumovirus Reinfection in Aged Mice Recapitulates Increased Disease Severity in Elderly Humans Infected with Human Metapneumovirus. Immunohorizons 7, 398–411 (2023). [PubMed: 37261717]
56. Misharin AV, Morales-Nebreda L, Mutlu GM, Budinger GRS & Perlman H Flow cytometric analysis of macrophages and dendritic cell subsets in the mouse lung. Am. J. Respir. Cell Mol. Biol 49, 503–510 (2013). [PubMed: 23672262]
57. Herring SE et al. Mitochondrial ROS production by neutrophils is required for host antimicrobial function against Streptococcus pneumoniae and is controlled by A2B adenosine receptor signaling. PLoS Pathog. 18, e1010700 (2022). [PubMed: 36374941]
58. Manni ML et al. Nitroalkene fatty acids modulate bile acid metabolism and lung function in obese asthma. Sci. Rep 11, 17788 (2021). [PubMed: 34493738]
59. Hantos Z, Daróczy B, Suki B, Nagy S & Fredberg JJ Input impedance and peripheral inhomogeneity of dog lungs. J. Appl. Physiol 72, 168–178 (1992). [PubMed: 1537711]
60. Ogishi M. et al. Impaired IL-23-dependent induction of IFN-γ underlies mycobacterial disease in patients with inherited TYK2 deficiency. J. Exp. Med 219, (2022).
61. Squair JW et al. Confronting false discoveries in single-cell differential expression. Nat. Commun 12, 5692 (2021). [PubMed: 34584091]
62. Philippot Q. et al. Human IL-23 is essential for IFN-γ-dependent immunity to mycobacteria. Sci. Immunol 8, eabq5204 (2023). [PubMed: 36763636]

Highlights

Respiratory viral infections remain a leading cause of death in young children. In the current study, we developed a model of human metapneumovirus (HMPV) infection in neonatal and adult mice. PD-1 limits unrestrained activation of cytotoxic T cells and thus is indispensable for preventing autoimmunity and infection-triggered immunopathology. We found that disruption of PD-1 signaling increased $CD8^+$ T cell functions and acute immunopathology with HMPV or influenza infection in neonates. Neonatal mice lacking PD-1 signaling also had longstanding changes in lung physiology. Surprisingly, adult mice with or without PD-1 controlled HMPV similarly without any signs of immunopathology. Together, these results demonstrate a critical regulatory role of PD-1 in limiting immunopathology from respiratory viral infections in neonates.

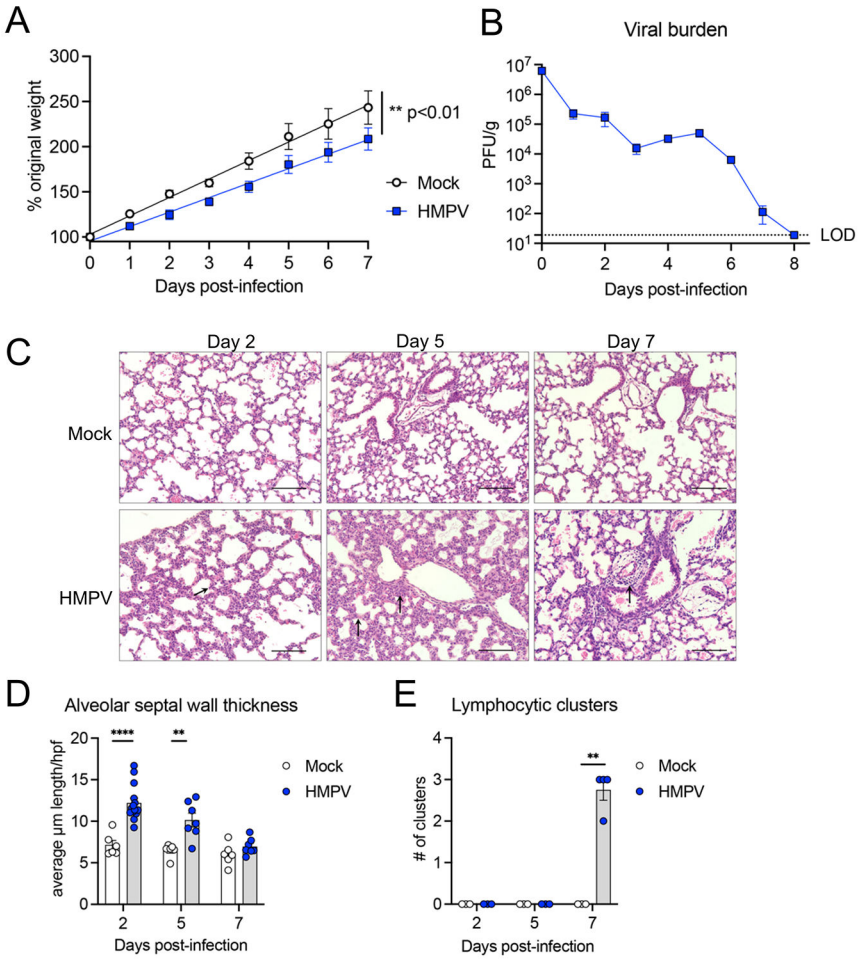

Figure 1. Establishment of neonatal model of human metapneumovirus (HMPV) infection.

A.) Neonatal C57Bl/6 mice infected with $2.8x10^6$ PFU of HMPV had significant reduction in rate of weight gain compared to co-housed, mock-infected controls as determined by simple linear regression modeling. Mock n=9, HMPV n=10, generated from three independent litters (n=3/group per litter). B.) Neonatal mice were permissive to HMPV infection but cleared viral burden by day 8 post-infection (performed on three litters with the following n/day: d0:1, d1:5, d2:2, d3:3, d4:5, d5: 4, d6:2, d7:4, d8:2). LOD denotes limit of detection. C.) H&E staining of HMPV infected or mock-infected lungs at day 2, 5, and 7 post-infection, with black arrows indicating interstitial inflammation, perivascular/peribronchial inflammation, and lymphocytic clusters at the respective time points. Scale bars indicate 100µm. D.) Quantification of average alveolar septal wall thickness (left) per high-powered field (hpf). **p<0.01, ****p<0.0005 by multiple t-tests. E.) Number of lymphocytic clusters per lung slice per animal at days 2, 5, 7, n=3-4 animals/group. **p<0.01 by multiple t-tests.

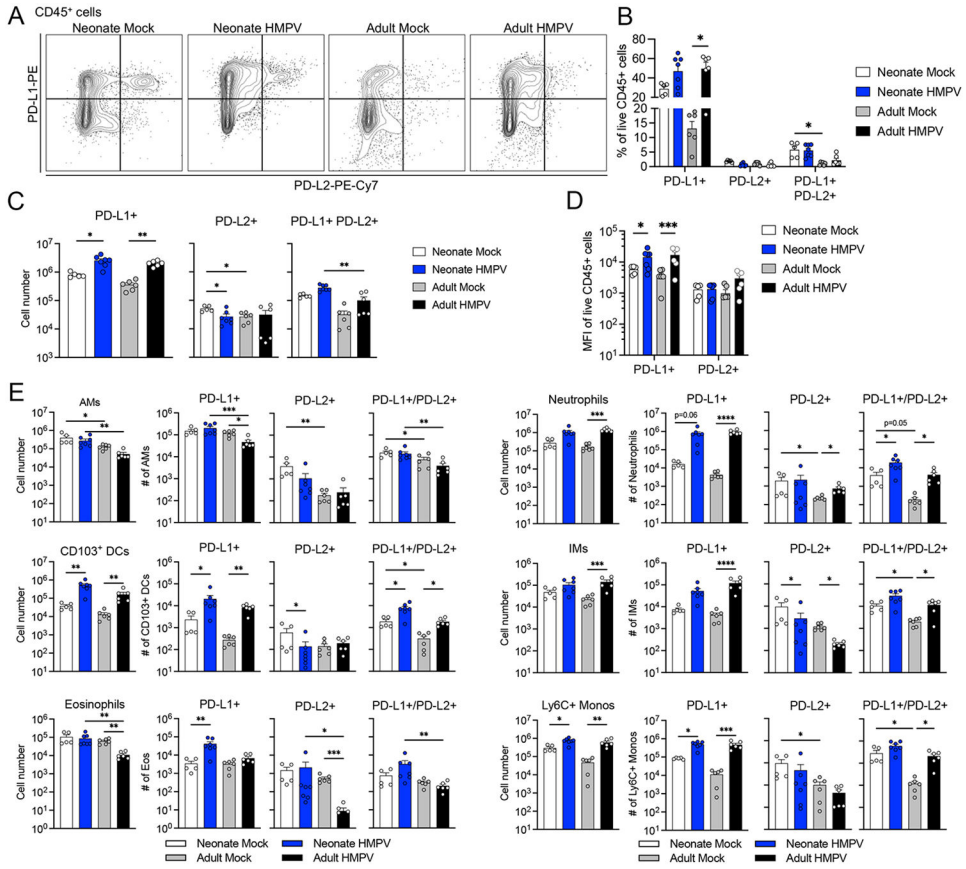

Figure 2. PD-L1/PD-L2 expression is upregulated following at day one post-HMPV infection in neonates.

A.) Representative flow plots of PD-L1 and PD-L2 expression on live CD45$^+$ cells one day after HMPV or mock infection in neonates/adults. B.) Proportion of CD45$^+$ cells expressing of PD-L1, PD-L2, PD-L1/PD-L2+ or PD-L1/PD-L2 negative by age/infection status. C.) Cell number of PD-L1, PD-L2, and PD-L1/PD-L2+ by age/infection status. D.) MFI of PD-L1 and PD-L2 by age/infection status. E.) Cell number of each cell subset, PD-L1+, PD-L2+, and PD-L1/PD-L2+ on alveolar macrophages (AMs), CD103$^+$ dendritic cells (DCs), eosinophils (Eos), neutrophils, interstitial macrophages (IMs), and Ly6C$^+$ monocytes (Monos). Neonate mock n=5, neonate HMPV n=7, adult mock n=6, adult HMPV n=6, experiments performed in duplicate with n=2-4/group. Statistical significance assessed by Kruskal-Wallis test, *p<0.05, **p<0.01, ***p<0.005, ****p<0.0005.

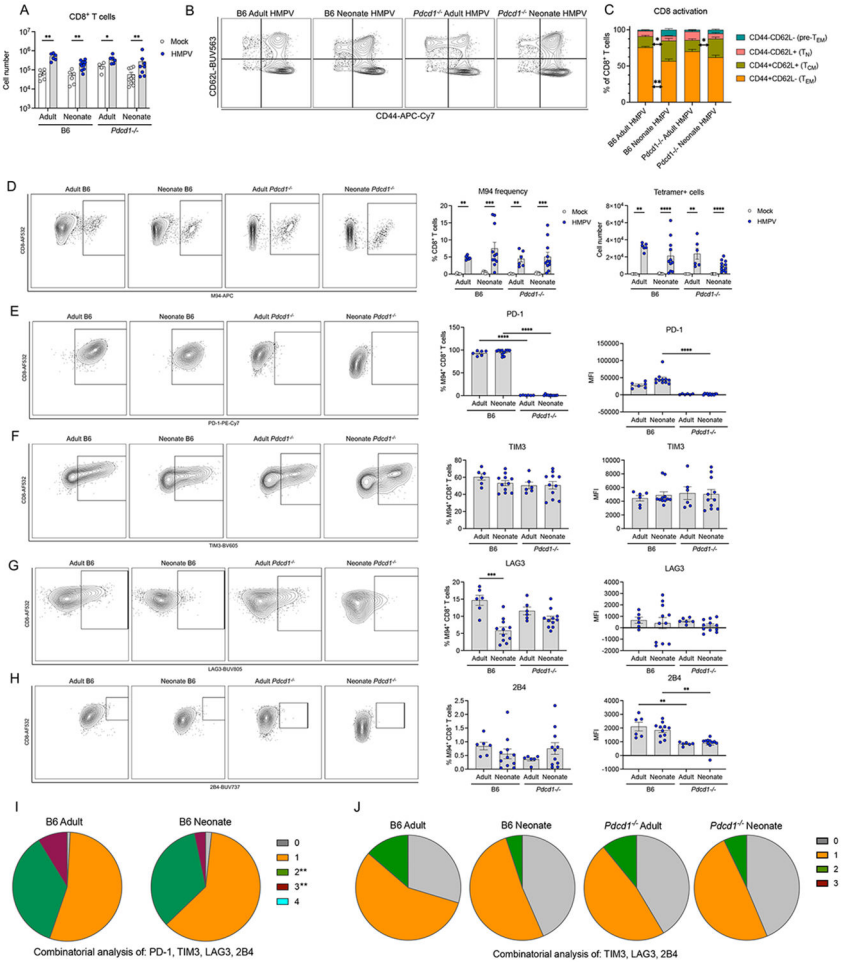

Figure 3. Neonatal CD8$^+$ T cells have a similar antigen-specific response by magnitude, but do not upregulate inhibitory receptors like adult CD8$^+$ T cells.

A.) CD8$^+$ T cell recruitment following HMPV infection at day 7 post-mock/HMPV infection. n per group, from left to right: 6; 6; 6; 11; 4; 6; 10; 8). Mock infected groups performed in duplicate, HMPV infected groups performed in triplicate. B.) Representative flow plots of CD44 and CD62L expression by age/genotype on CD8$^+$ T cells following HMPV infection. C.) Combined analysis of CD44 and CD62L expression by age/genotype following HMPV infection. *p<0.05, **p<0.01 by two-way ANOVA with multiple comparisons. n=6 for adult groups, n=11 for B6 and n=11 for *Pdcd1*$^{-/-}$ neonatal groups. D.) Representative flow plots of M94-tetramer staining with composite M94 frequency and cell number. n per group, from left to right: 6; 6; 6; 11; 4; 6; 11; 8. Mock infected groups performed in duplicate, HMPV infected groups performed in triplicate Representative flow plots, M94$^+$ tetramer frequency, and MFI to measure expression of PD-1 (E), TIM3 (F), and LAG3 (G) and 2B4 (H). n=6 for adult groups, n=11 for B6 and n=11 for *Pdcd1*$^{-/-}$ neonatal groups with adult groups performed in duplicate and neonate performed in triplicate (n=3-4/experiment) *p<0.05, **p<0.01, ****p<0.0005 by Kruskal-Wallis test. I.) Boolean gating analysis of expression of four inhibitory receptors, with **p<0.01 by two-way ANOVA with multiple comparisons. J.) Boolean gating analysis excluding PD-1 expression.

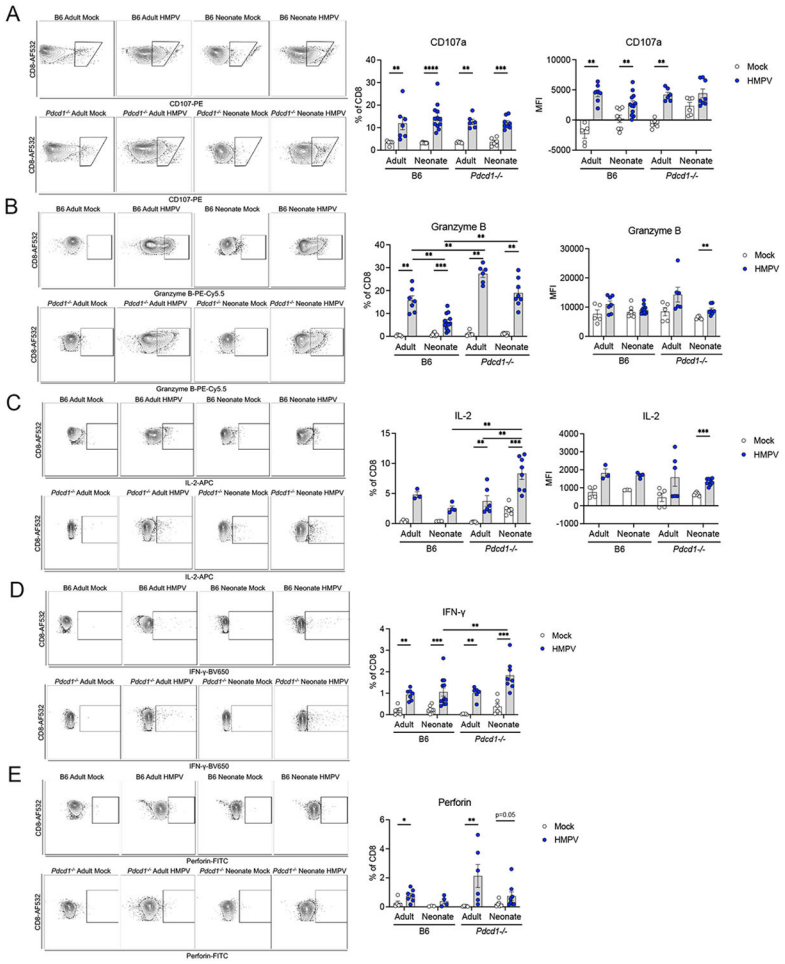

Figure 4. Neonatal mice have reduced effector function, which is restored in the absence of PD-1.

Effector function was assessed in $CD8^+$ T cells at day 7 post-infection. A.) Representative flow plots of surface CD107a expression per infection status, genotype, and age. Frequency of % $CD107a^+$ and CD107a MFI demonstrated to the right. Mock groups: B6 adult (n=5), B6 neonates (n=8), *Pdcd1*$^{-/-}$ adult (n=5), *Pdcd1*$^{-/-}$ neonates (n=6); HMPV groups: B6 adult (n=7), B6 neonates (n=12), *Pdcd1*$^{-/-}$ adult (n=6), *Pdcd1*$^{-/-}$ neonates (n=8). All experiments performed in triplicate. B.) Representative flow plots of granzyme B expression per infection status, genotype, and age, with frequency and MFI demonstrated to the right. Mock groups: B6 adult (n=5), B6 neonates (n=8), *Pdcd1*$^{-/-}$ adult (n=5), *Pdcd1*$^{-/-}$ neonates (n=6); HMPV groups: B6 adult (n=7), B6 neonates (n=12), *Pdcd1*$^{-/-}$ adult (n=6), *Pdcd1*$^{-/-}$ neonates (n=8). All experiments performed in triplicate. C.) Representative flow plots of IL-2 expression per infection status, genotype, and age, with frequency and MFI demonstrated to the right, n=4-8 for neonatal infection groups. Mock groups: B6 adult (n=4), B6 neonates (n=3), *Pdcd1*$^{-/-}$ adult (n=5), *Pdcd1*$^{-/-}$ neonates (n=6); HMPV groups: B6 adult (n=3), B6 neonates (n=4), *Pdcd1*$^{-/-}$ adult (n=6), *Pdcd1*$^{-/-}$ neonates (n=7). D.) Representative flow plots and frequency of IFN-γ expression per infection status, genotype, and age. Mock groups: B6 adult (n=5), B6 neonates (n=8), *Pdcd1*$^{-/-}$ adult (n=5), *Pdcd1*$^{-/-}$ neonates (n=6); HMPV groups: B6 adult (n=7), B6 neonates (n=12), *Pdcd1*$^{-/-}$ adult (n=6), *Pdcd1*$^{-/-}$ neonates (n=8). All experiments performed in triplicate. E.) Representative flow plots and

frequency of perforin expression per infection status, genotype, and age. Mock groups: B6 adult (n=5), B6 neonates (n=3), *Pdcd1*$^{-/-}$ adult (n=5), *Pdcd1*$^{-/-}$ neonates (n=6); HMPV groups: B6 adult (n=7), B6 neonates (n=4), *Pdcd1*$^{-/-}$ adult (n=6), *Pdcd1*$^{-/-}$ neonates (n=8). Statistical significance assessed by Kruskal-Wallis test, *p<0.05, **p<0.01, ***p<0.005, ****p<0.0005.

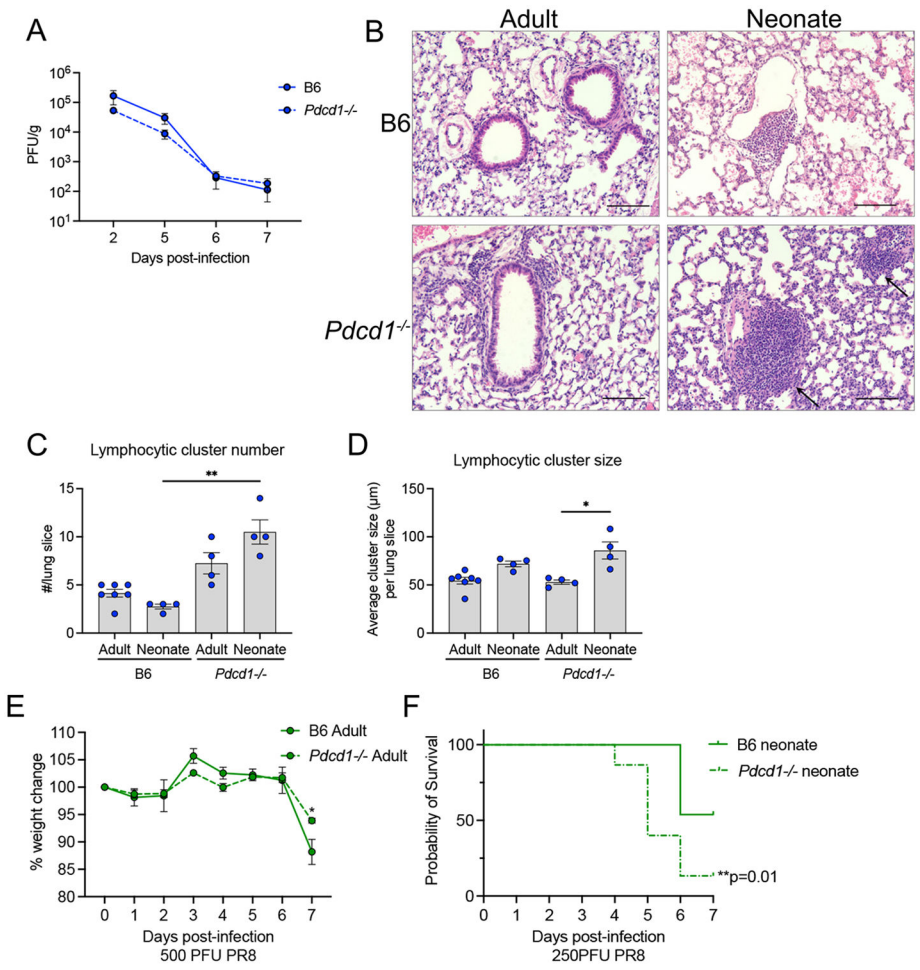

Figure 5. Neonatal mice lacking PD-1 had increased acute pathologic features following respiratory viral infection.

A.) Similar HMPV clearance kinetics in B6 and *Pdcd1*$^{-/-}$ mice (B6 n/day: d2:2, d5:7, d6:3, d7:4; *Pdcd1*$^{-/-}$ n/day: d2:2, d5:6, d6:4, d7:7, performed on three total litters). B.) Increased lymphocytic cluster size demonstrated by black arrows at 7 post-infection in *Pdcd1*$^{-/-}$ neonates, with residual inflammation noted in B6 adults, B6 neonates, and *Pdcd1*$^{-/-}$ adults. Scale bars indicate 100μm. C.) Number of lymphocytic clusters per lung slice. **p<0.01 by Kruskal-Wallis test (n=4-7/group). D.) Quantification of average lymphocytic cluster size per lung slice, *p<0.05 by Kruskal-Wallis test (n=4-7/group). E.) *Pdcd1*$^{-/-}$ adult mice (n=6) showed decreased weight loss at day 7 after PR8 infection compared to B6 adults (n=4,*p<0.05 by multiple t-tests). F.) *Pdcd1*$^{-/-}$ neonates (n=15) had increased mortality following influenza infection when compared to B6 neonates (n=13). Survival analysis performed, **p=0.01.

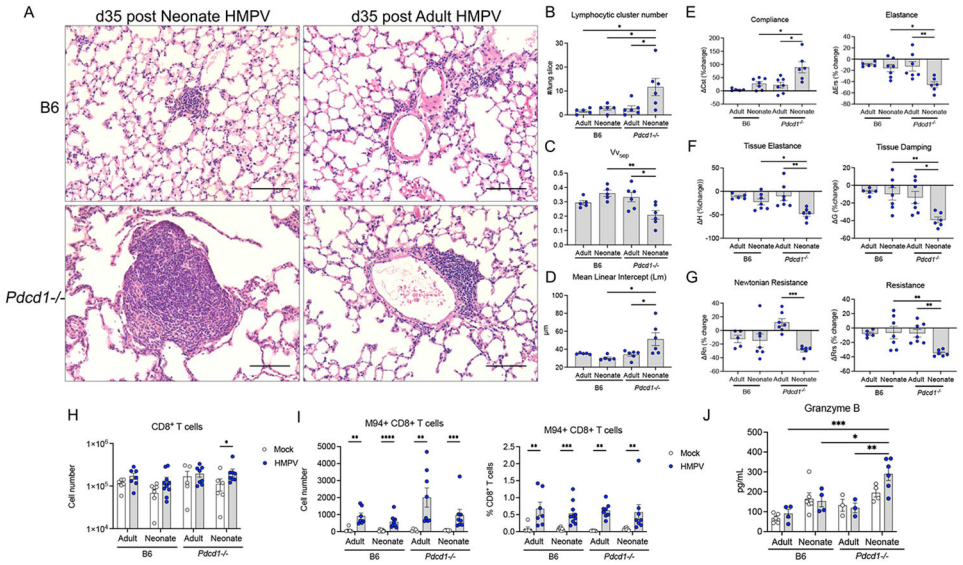

Figure 6. Neonatal mice lacking PD-1 infected with HMPV have chronic lung changes and CD8$^+$ activation.

A.) H&E demonstrating increased lymphocytic aggregates and abnormal alveolar architecture in *Pdcd1*$^{-/-}$ mice infected with HMPV as neonates, but not B6 neonates or *Pdcd1*$^{-/-}$ adults, 35 days following HMPV infection. Scale bars indicate 100μm. B.) Number of lymphocytic clusters per lung slice per animal (n=5-6/group). C-D.) Septal volume density (Vv_{sep}) and mean linear intercept per lung slice per animal (n=5-6/group). E.) Thirty-five days following neonatal HMPV infection, *Pdcd1*$^{-/-}$ mice had altered compliance (Cst) and elastance (Ers) compared to B6 mice as measured by flexiVvent. F.) Tissue elastance (H) and tissue damping (G) were significantly reduced in *Pdcd1*$^{-/-}$ mice infected as neonates. G.) Altered resistance (Rrs, Rn) patterns in *Pdcd1*$^{-/-}$ mice infected with HMPV as neonates. Data are presented as percent change ((HMPV-mock)/mock)*100 with the average of mock-infected littermate controls serving as the mock measurement. Sample sizes for HMPV infected groups: adult B6=5, neonatal B6=7, adult *Pdcd1*$^{-/-}$=7, and neonatal *Pdcd1*$^{-/-}$=6. Mock infected groups: adult B6=5, neonatal B6=10, adult *Pdcd1*$^{-/-}$=7, and neonatal *Pdcd1*$^{-/-}$=4 Performed in duplicate with n=2-5/experiment. H.) CD8$^+$ T cell number by genotype, age at infection (i.e. neonatal vs. adult), and infection status (i.e. mock vs. HMPV) at 35 days post-infection. n per group, from left to right: 6; 7; 7; 10; 5; 8; 6;8,performed in duplicate with n=2-5 per experiment I.) Cell number and frequency of M94$^+$ CD8$^+$ T cells at day 35 post-infection. n per group, from left to right: 6; 7; 7; 10; 5; 8; 6; 8, performed in duplicate with n=2-5 per experiment J.) Granzyme B protein level as measured by ELISA in lung homogenate at day 35 post-infection. n per group, from left to right: 5; 4; 6; 4; 3; 3; 4; 6. Statistical analysis was performed using a Kruskal-Wallis test for comparisons across HMPV infected group. Multiple Mann-Whitney tests were utilized to compare mock vs. HMPV-infected for an individual age/genotype. *p<0.05, **p<0.01, ***p<0.005, ****p<0.0005

Table 1.

Summary of differences between neonatal and adult mice at baseline and following infection with human metapneumovirus.

	B6 neonates vs B6 adults	***Pdcd1*$^{-/-}$ neonates vs *Pdcd1*$^{-/-}$ adults**	***Pdcd1*$^{-/-}$ neonates vs B6 neonates**
Baseline differences			
CD107a MFI (degranulation)	↑	↔	↔
ROS production	↑	N/A	N/A
CD8$^+$T cell responses to HMPV			
Antigen-specific CD8$^+$ formation	↔	↔	↔
LAG3 upregulation	↓	↔	↔
Multiple inhibitory receptors	↓	↔	↔
Granzyme B production	↓	↔	↑
IL-2 production	↔	↑	↑
Acute pathology following respiratory viral infection			
Lymphocytic cluster formation after HMPV	↔	↑	↑↑
Mortality after influenza challenge	↑	↑	↑↑
Chronic pathology following respiratory viral infection			
Lymphocytic cluster formation	↔	↑↑	↑↑
Abnormal alveolar architecture (i.e., alveolar simplification)	↔	↑↑	↑↑
Lung compliance	↔	↑	↑
Lung elastance	↔	↓	↓
Airway resistance	↔	↓	↓
Granzyme B production 35 days post-HMPV infection	↔	↑	↑